

Time Transients with Inductive Loop Traces in Metal Halide Perovskites

Enrique Hernández-Balaguera* and Juan Bisquert

Metal halide perovskites are archetypal ionic-electronic materials with great prospects for optoelectronic applications. Among the rich variety of physics exhibited by ionic-electronic conduction, here, those most relevant to optoelectronic devices in which ionic mechanisms introduce a kinetic delay in the electronic phenomena are analyzed. The attention is focused on the inductive loop features and a dynamical model is developed to describe the corresponding complex multiscale dynamics in the time domain under experimental conditions, finally explaining the fundamental structure of the current transient responses in halide perovskite semiconductors. Based on complex capacitive and inductive patterns extensively studied in impedance measurements, an adequate interpretation of time domain methods capable of monitoring charge-carrier dynamics is produced. Therefore, this methodology identifies the characteristic parameters of all types of transient dynamics in metal halide perovskites, providing a suitable connection of correlated techniques, including impedance and chronoamperometric experiments, toward a robust interpretation of the device response. The scope of the method is fairly general, since these counterintuitive transient effects are observable not only in metal halide perovskites, but also in multiple materials and processes, mainly in different research fields pertaining to electrochemistry and electronics.

This semiconducting material creates rich and surprising physical phenomena that have required advances in fundamental understanding to drive rapid development.^[2–4] Most of the widely reported strange phenomenology has been associated with the soft nature of the metal halide perovskites' crystal structure which allows migration of structural ionic defects,^[5,6] becoming hence combined with the electronic transport that happens naturally in the semiconductor. Ionic-electronic conductors span a huge variety of materials and systems and their electrical properties are often difficult to determine, since ionic and electronic carriers respond combinedly to the external perturbations.^[7–11] In the analysis of metal halide perovskites, the situation is even more complicated by the presence of recombination and chemical transformation phenomena.^[12–14] In this context, Impedance Spectroscopy has been a key asset to analyze these mixed ionic-electronic processes,^[15] even though obtaining a univocal interpretation of the complex plane plots was elusive in the initial years of investigation compared to the success

story of this experimental technique applied in other electronic devices.^[16–19] Thus, time transient techniques, one of the most important and equally valid alternative approaches to device modeling, involve much more challenging access to all the different electronic and ionic processes taking place simultaneously.


The use of time-resolved relaxation analysis represents a very popular characterization tool in materials sciences and specifically in the field of perovskite semiconductors,^[20–24] also aiming to explain the dynamic processes governing the device response under small- or large-signal conditions. Although there is a clear connection with the frequency domain via Laplace transform methods in the first case, the transformation is not always trivial, leading to uncertainties about the interpretation of the results, especially due to a number of unexpected phenomena (such as negative spike components and mixed capacitive-inductive dynamics)^[21,25–27] that lead to multiple transient shapes such as those studied here. For a large perturbation, models include nonlinear elements, so they are not appropriate for dealing with impedance data. At this point, a question naturally arises as to why one would use a more complex methodology for interpreting experimental data as time transient methods instead of the well-established technique of Impedance Spectroscopy in

1. Introduction

Metal halide perovskites have generated widespread interest in the international community over the past few years, opening up a new avenue for the next generation of optoelectronic devices.^[1]

E. Hernández-Balaguera
Escuela Superior de Ciencias Experimentales y Tecnología
Universidad Rey Juan Carlos
C/ Tulipán, s/n, Móstoles, Madrid 28933, Spain
E-mail: enrique.hernandez@urjc.es

J. Bisquert
Institute of Advanced Materials (INAM)
Universitat Jaume I
Castelló 12006, Spain

 The ORCID identification number(s) for the author(s) of this article can be found under <https://doi.org/10.1002/adfm.202308678>

© 2023 The Authors. Advanced Functional Materials published by Wiley-VCH GmbH. This is an open access article under the terms of the Creative Commons Attribution-NonCommercial License, which permits use, distribution and reproduction in any medium, provided the original work is properly cited and is not used for commercial purposes.

DOI: 10.1002/adfm.202308678

materials science characterization for several decades.^[28,29] The answer follows directly from the monitoring of charge-carrier dynamics in the context of the inherent memory effects extensively observed in these material classes.^[30] Impedance measurements are carried out on a particular steady-state determined by a dc voltage bias (no memory). In contrast, time-domain analysis allows us to handle adequately the past history of the device from the initial conditions and thus, for example, to control the undesired effects of current–voltage hysteresis in photovoltaic applications^[3,31–33] or understand the temporal evolution of the conductance states as a fundamental operation for in-memory computing.^[34,35] Another fundamental advantage of chronoamperometric experiments, in comparison to the familiar technique of Impedance Spectroscopy, basically includes ultrahigh speed data acquisition to real-time monitor current evolution during voltage scans, satisfying the time-invariant assumption of these highly unstable materials and decelerating potential degradation pathways in the devices.

Beyond the capacitive arcs observed frequently in optoelectronic devices, metal halide perovskites also exhibit, in the impedance plots, inductive features whose corresponding capacitances result in negative values. This characteristic impedance pattern has been a matter of general interest due to the complexity of associating a specific circuit element (light-enhanced and negative capacitance^[26] or chemical inductor)^[36] to such a concrete physical process not only in the devices under study here, but also in previously reported electrochemical and electronic phenomena.^[37–40] In perovskite materials with semiconductor properties, it exists two inductive-type spectral behaviors according to the literature; intermediate loops or spiraling features between the high- and low-frequency capacitive arcs^[41,42] and final semicircles, in the form of hooks or curl-backs in the fourth quadrant, at long time scales.^[43–45] Both anomalous features involve a common kinetic origin associated to the ionic-electronic accumulation at the interfaces that influences the charge transfer and recombination mechanisms. The difference between these two impedance responses arises, quantitatively speaking, from the delay, between the overall current response (output) and the voltage imposed (input), induced by the changing environment of ions.^[15,36,42] Depending on the time-delay value, the inductance will manifest itself earlier (loops and spirals) or later (hooks and curl-backs) in the impedance responses, even though the equivalent circuit is the same for these different scenarios. Recently, the authors extensively provided a basic picture of the shape of time transients when the chemical inductor appears at the low-frequency end of the spectrum,^[27] requiring now a dedicated and systematic approach that includes intermediate frequency loops.

In the literature, it has been extensively observed the transient current response, due to inductive loop effects found by Impedance Spectroscopy, in response to step voltages for devices based on metal halide perovskite materials. As a representative example, **Figure 1a** shows the results of chronoamperometry experiments of perovskite solar cells, after jumping from the equilibrium condition to different voltage values, in the dark. When the voltage is switched from 0 V to values higher than 0.9 V, current transient responses show complex multiscale dynamics with a clear physical meaning correlated with electron/hole displacement currents (spike at $t = 0$), competing recombination pathways (minimum 1) and a compensated electric field due to

slow ionic motion (minimum 2).^[25] On the other hand, **Figure 1b** shows a similar current evolution with time in perovskite solar cells in the range of high voltage values.^[46] After the classical capacitive decrease, another dynamical transient behavior appears in which the current response increases and then decreases with time; that is, an N-shape curve. This type of current time transients, with multiple spikes and changing dynamics, have been amply reported in different technologies of metal halide perovskites, but in most of the cases, the numerical simulations fail to reproduce the resulting current transient behavior (e.g., see **Figure 1b**). For this reason, it is necessary to develop a general dynamical model for a quantitative description and interpretation of this ubiquitous dynamics observed in perovskite semiconductors over more than a decade.

In this work, we track the different features of the transient dynamics in metal halide perovskite devices due to inductive loops in impedance measurements. Although the physical explanation associated to this pertinent feature has been adequately traced by Impedance Spectroscopy, the situation is far from being completely formulated across different measurement protocols. We here aim to explain the multiple transitions of these types of transient responses under small-signal conditions, interchanging continuously capacitive and inductive patterns with time. In this scenario in which the chemical inductor emerges at intermediate frequencies, the temporal evolution of the current indeed undergoes a rectification in the decay pattern at specific operating points along the current–voltage characteristics, thus containing significant information about dynamics that affect the determination of the device performance. As experimental results, we use a representative example of metal halide perovskites acting as a solar cell. To analyze the transient dynamics in perovskite semiconductors from a general perspective, we present a summary for the adequate estimation of the characteristic parameters in the complex time responses by using basic concepts of circuit theory.

2. Results and Discussion

2.1. Visualization of the Inductive Loop in the Impedance Response of Perovskite Semiconductors

Often, the impedance response in perovskite semiconductors exhibits the curious feature that the spectra turn, after outlining a high-frequency capacitive arc, to positive imaginary values (inductive mechanisms), as indicated in **Figure 2a**, to finally retrace a slow capacitive semicircle at high bias voltages (here, 1 V in dark conditions). Note that the spectra have been measured in perovskite solar cells consisting of fluorine-doped tin oxide (FTO)/compact titanium dioxide (c-TiO₂)/mesoporous titanium dioxide (m-TiO₂)/multiplication perovskite absorber with composition Cs_{0.05}MA_{0.15}FA_{0.80}Pb_{1.05}(I_{0.85}Br_{0.15})_{3/2,2',7,7'}-Tetrakis[N,N-di(4-methoxyphenyl)amino]–9,9'-spiro-bifluorene (spiro-OMeTAD)/Au device structure, with power conversion efficiencies approaching 19%. With respect to the stoichiometric composition of perovskites, we add an excess of Pb content in the precursor solutions to improve the efficiency and stability of our solar cells for exposure to prolonged illumination.^[47,48] Further details of device fabrication and characterization are described in Supporting Information. Alternatively, we show

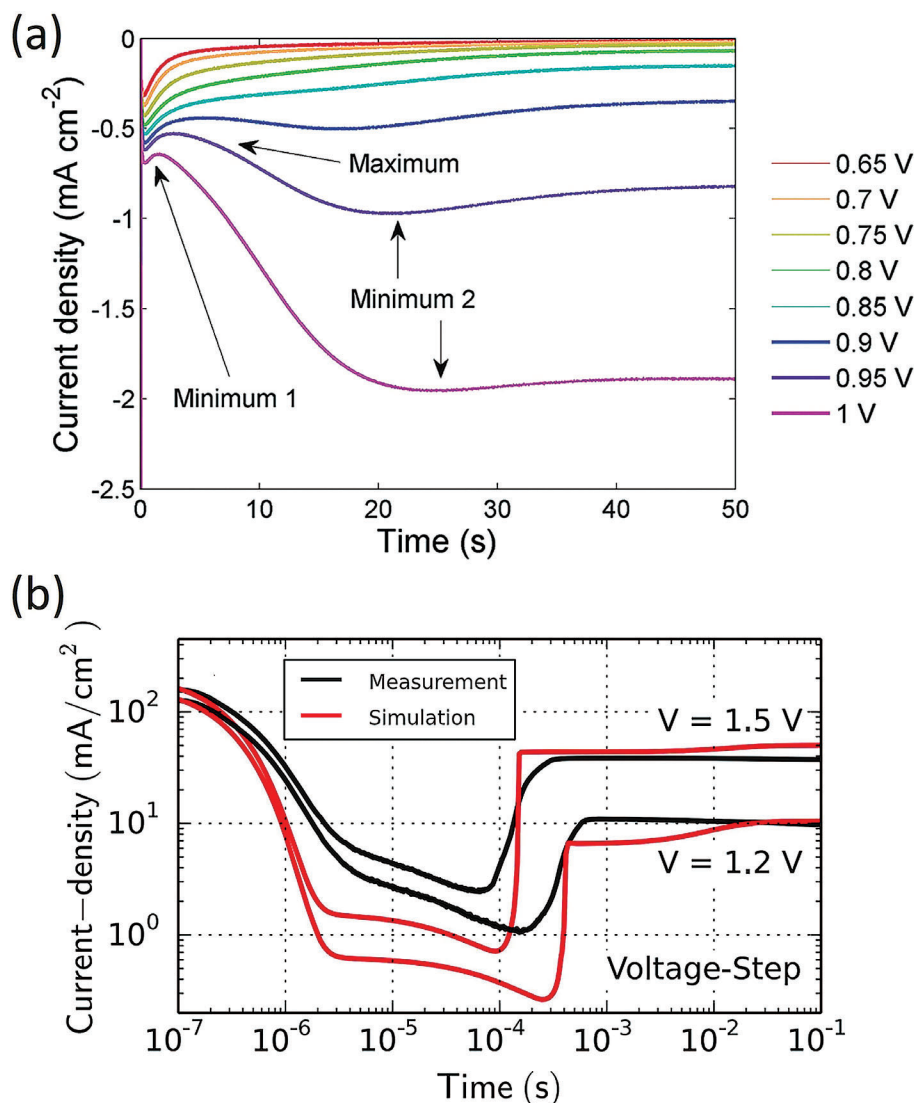


Figure 1. a) Experimental evolution of current transients in response to steps from 0 V to different values of voltage for a perovskite solar cell with configuration FTO/TiO₂/MAPI/spiro-OMeTAD/Au cell. Reproduced from Ref. [25] (Royal Society of Chemistry, 2017). Time transient with inductive loop traces appears at voltage values higher than 0.9 V. b) Measurement (black) and simulation (red) of transient currents as a response to voltage steps in the dark in the log-log representation for a device structure as ITO/TaTm:F₆-TCNNQ/TaTm/MAPI/C₆₀/C60:PhIm/Ag. Reproduced from Ref. [46] (American Chemical Society, 2019).

the important representation of the frequency-dependent capacitance in the Bode plot representation (see Figure 2b). This rephrasing of the impedance data traces a transition between two capacitive plateaus, providing negative values with undershoots in the middle-frequency range, associated to the inductive loop observed in impedance.^[42,49] These relaxation processes, underlying physical properties, are represented by the different elements of the equivalent circuit shown in Figure 2c, where R_s is the parasitic series resistance, R_b and R_a are the two branches of the recombination resistance, while R_x is the resistance for ionic relaxation.^[17,50] C_g denotes the dielectric capacitance, L_a the chemical inductance, and C_x the interfacial charging capacitance. The electrical model of Figure 2c constitutes the most successful equivalent circuit for the impedance response since it exploits, in a universal and physically motivated way, the

rich variety of ambiguous perovskite patterns found through Impedance Spectroscopy.^[27,51,52] Nevertheless, it is necessary to clarify that not all the components of this electrical model are present in the entire voltage range and all types of samples. Next, we study the correspondent time transient dynamics.

In accordance with the complexity of the general equivalent circuit of Figure 2c extracted by using impedance measurements with the following impedance,

$$Z(\omega) = R_s + \left[j\omega C_g + \frac{1}{R_b} + \frac{1}{R_a + j\omega L_a} + \frac{1}{R_x + \frac{1}{j\omega C_x}} \right]^{-1} \quad (1)$$

we can predict the small-perturbation time-domain current response $\Delta j(t)$ around a steady-state value, in the sense of a 3D

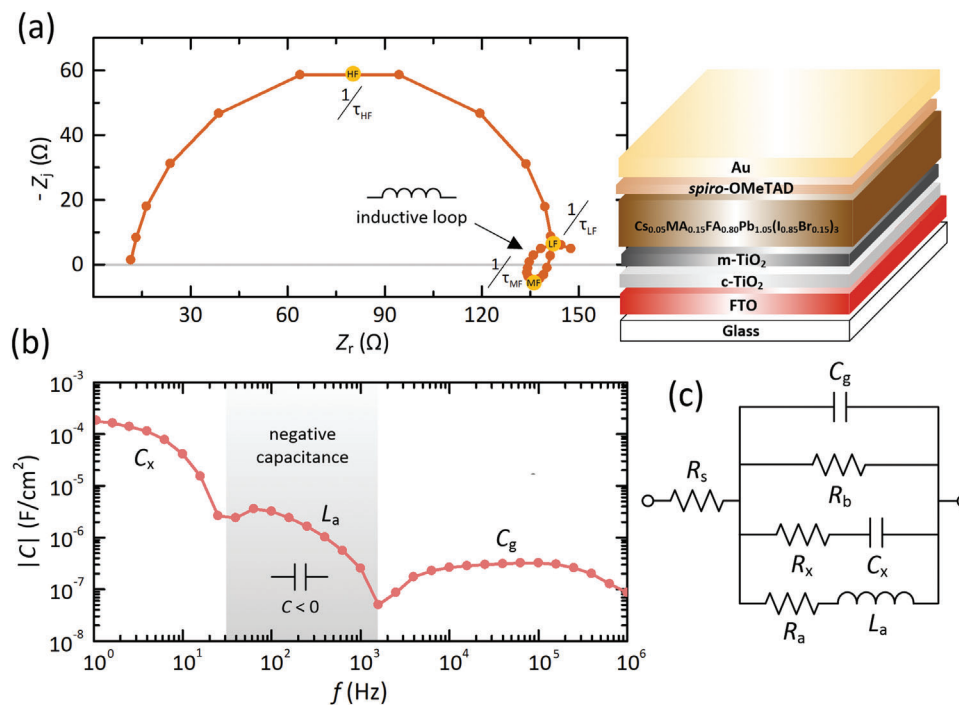


Figure 2. a) Complex impedance plane (characteristic frequencies marked) and b) capacitance-frequency plot (negative values shaded) of the cesium-containing triple-cation perovskite device under study here in the dark conditions and with an applied voltage bias of 1 V. c) Equivalent circuit used for spectra with two capacitive processes and inductive traces at intermediate frequencies, with the branches in parallel. $Z_r(\omega)$ and $Z_i(\omega)$ are the real and imaginary parts of the impedance, C is the capacitance, and ω is the frequency.

model, from the following dynamical system of linear differential equations:

$$\Delta j(t) = C_g \frac{d(\Delta V(t))}{dt} + \frac{\Delta V(t)}{R_b} + \Delta j_L(t) + C_x \frac{d(\Delta V_s(t))}{dt} \quad (2)$$

$$\tau_L \frac{d(\Delta j_L(t))}{dt} = \frac{\Delta V(t)}{R_a} - \Delta j_L(t) \quad (3)$$

$$\tau_C \frac{d(\Delta V_s(t))}{dt} = \Delta V(t) - \Delta V_s(t) \quad (4)$$

In Equations (2)–(4), the currents and voltages bear the difference operator Δ since they correspond to small amplitude quantities. On the one hand, $\Delta j(t)$ and $\Delta V(t)$ determine the voltage and current, respectively, of the device and, on the other hand, $\Delta j_L(t)$ and $\Delta V_s(t)$ represent the internal state variables related to the current passing through the chemical inductor and the voltage across the light-enhanced capacitance, respectively. These internal state variables emerge naturally throughout a current–voltage curve (stepwise scan) with their own relaxation effects,^[53] resulting in the essential memory properties of the metal halide perovskites by slow recoveries of relaxation times for Equations (3) and (4), respectively,

$$\tau_L = \frac{L_a}{R_a} \quad (5)$$

$$\tau_C = R_x C_x \quad (6)$$

in response to changes, by voltage-driven adaptation functions (right-hand sides of Equations (3) and (4)).^[54–56] Note that Equations (5) and (6) provide characteristic times of the same order ($\tau_L \sim \tau_C$)^[52,55] but different from those of the impedance relaxation processes (inverse of the frequencies): $\tau_{HF} = (1/R_b + 1/R_x)^{-1} C_g$, $\tau_{MF} = [L_a/(1/R_b + 1/R_x)^{-1} + R_a]$, and $\tau_{LF} = [R_x + (1/R_b + 1/R_a)^{-1}] C_x$ at high, medium, and low frequencies, respectively. This theory is derived from a general dynamical framework, described in Supporting Information.

As a final remark, it should be mentioned that device modeling, based on impedance measurements, provides just a global and approximate representation of the dominant physical processes at each steady-state situation. The relaxation patterns of metal halide perovskites are commonly too complex for a simple impedance analysis with potential weaknesses such as ambiguity, “over-parameterization” or incompatibility with nonlinear elements.^[15,57] For accurate modeling of the device operation, it is essential to include more than one technique to bring light to the intricate nature of the response in metal halide perovskites. Next, we give a complete picture of such capacitive-inductive processes through time-transient methods that contribute to the measured impedance.

2.2. Inductive Loop Effects in Current Transients with Complex Multiscale Dynamics

Generally, the electrical response of metal halide perovskites exhibits a recognizable pattern of two to three processes when the

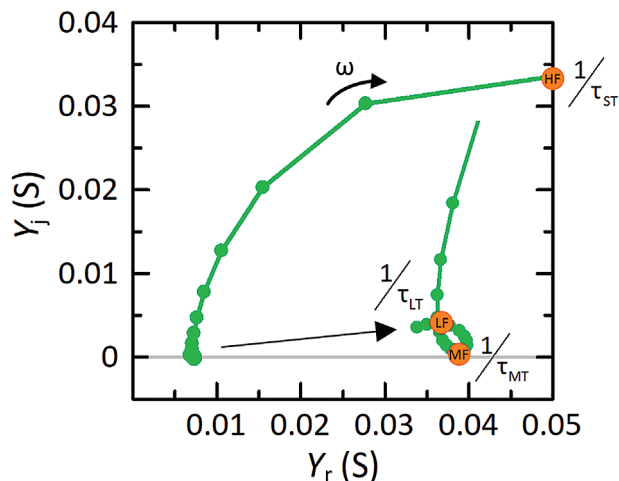


Figure 3. Admittance spectra calculated from the impedance response of Figure 2a.

voltage is scanned as in the measurement of a current–voltage curve.^[15,16,18,58] The slow dynamical behavior primarily governs the transient dynamics due to interfacial phenomena that represent a foremost feature of these optoelectronic devices. In effect, the characteristic time of the fast variable τ_{ST} is much lower than that of the variable at intermediate times τ_{MT} and that of the slow ones, τ_{LT} . Accordingly, it is expected the property $\tau_{MT}, \tau_{LT} \gg \tau_{ST}$ of the metal halide perovskites.^[27,59] In perovskite electronics, τ_{ST} always is a capacitive time constant associated to the charging process of C_g . However, the origin of τ_{MT} and τ_{LT} can be interchanged due to capacitive or inductive processes (see below).

Now that we have named the main parameters of the transient current response (equivalent circuit, memory variables, and time constants), the question is how to obtain the analytical form of the current response $\Delta j(t)$. This question has two parts: First, is impedance function really the best form of immittance to extract the time constants of $\Delta j(t)$? The answer is negative because the transient response under analysis is a current (potentiostatic experiment) and, from a theoretical point of view, the impedance is a current-controlled function (in a galvanostatic manner): $Z(\omega) = \tilde{V}(\omega)/\tilde{j}(\omega)$. Therefore, it is necessary to transform the immittance spectroscopy data into an admittance response, $Y(\omega) = \tilde{j}(\omega)/\tilde{V}(\omega)$.^[33,60] Note that tildes indicate small oscillating voltage and currents. The admittance function, measured in Siemens, can be also represented in terms of the real and imaginary parts, $Y(\omega) = Y_r(\omega) + jY_j(\omega)$, where $Y_r(\omega)$ and $Y_j(\omega)$ are connected to the conductivity (conductance) and capacitive/inductive (susceptance) contributions.

To provide an adequate interpretation of the admittance response in this work, we show the equivalent spectra of Figure 2a in **Figure 3**. The important point to note here is that, as in an impedance diagram, the experimental data at which the admittance data cut the real axis represent the value of the resistances shown in the equivalent circuit (see Figure 2c). These similarities in the concepts and shape of impedance and admittance spectra lead to the second part of the question: What happens with the

values of the characteristic relaxation times? From a general perspective, we can obtain the value of the time constants of the current response by inspection as $\tau = R_{th} C$ and $\tau = L/R_{th}$, where R_{th} is the Thévenin resistance. Depending on the order of appearance of the capacitive and inductive effects, as indicated in Figure 3, the expressions of the time constants, again the inverse of the characteristic frequencies, will differ with respect to other inductive features (see below). First, the value of the fast time constant, ascribed to the dielectric capacitance, is given by:^[27,33,59]

$$\tau_{ST} = \left(\frac{1}{R_s} + \frac{1}{R_b} + \frac{1}{R_x} \right)^{-1} C_g \sim R_s C_g \quad (7)$$

because we consider, for simplicity, that there exists a substantial difference in the value of resistances of the electrical circuit at high bias voltages, and thus series resistance effects can be suppressed and considered negligible in the transient analysis, $R_s \rightarrow 0$. The resistance “seen” by C_g is determined under the assumption that the chemical inductor and the interfacial charging capacitance are discharged (virtual open- and short-circuits, respectively).

The sequence of processes in metal halide perovskites, when two or three phenomena with inductive characteristics emerge in Nyquist plots, can be summarized as capacitive-inductive-capacitive (CLC, loops and spirals) or capacitive-capacitive-inductive (CCL, hooks and curl-backs) ordered from the highest frequency feature to the lowest. Thus, the value of τ_{MT} and τ_{LT} will be exchanged. Note that, in effect, a pure chemical inductor at low frequencies is considered to be of the CCL type. For the case under study here concerning inductive loops (CLC), the value of the intermediate relaxation time is:

$$\tau_{MT} = \frac{L_a}{R_a + \left(\frac{1}{R_s} + \frac{1}{R_b} + \frac{1}{R_x} \right)^{-1}} \sim \frac{L_a}{R_a} \quad (8)$$

because now, in the Thévenin resistance, $R_a \gg (1/R_s + 1/R_b + 1/R_x)^{-1}$. Similarly, the characteristic parameter at long time scales results:

$$\tau_{LT} = \left[R_x + \left(\frac{1}{R_s} + \frac{1}{R_b} + \frac{1}{R_a} \right)^{-1} \right] C_x \sim R_x C_x \quad (9)$$

as the product of C_x and R_{th} “seen” to the left of the capacitor, by shorting the voltage input and making series and parallel combinations of the resistances, $(1/R_s + 1/R_b + 1/R_a)^{-1} \ll R_x$. In effect, $\tau_{MT} \sim \tau_L$ and $\tau_{LT} \sim \tau_C$, here. Here, we remark on the prominent difference between the characteristic time scales of the impedance and admittance functions (see above). Then, how can the electrical processes be separated in the experimental admittance response if $\tau_L \sim \tau_C$? This is due to slight experimental differences and the term associated with the parallel connection of resistances found in Equations (8) and (9), in addition to the fact that, with frequency domain techniques, it is possible to readily separate the physical processes.^[15] Although the parasitic series resistance is small and negligible in transient analysis, it introduces slight changes at lower and higher values in τ_{MT} and τ_{LT} , separating the processes and making it possible to visualize them in the frequency domain. This situation could lead to a

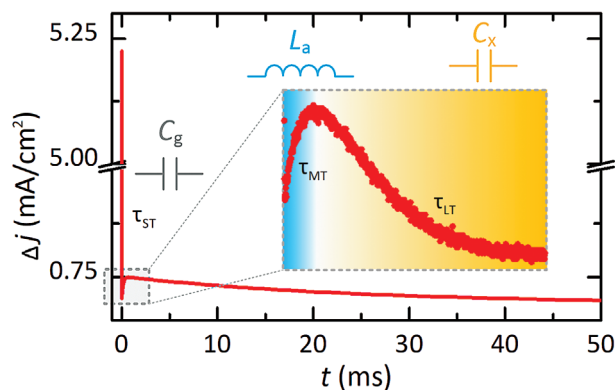


Figure 4. Transient current response at 1 V after applying a voltage step of +10 mV in the dark. The inset shows a zoomed-in view of the dynamical behavior with an inductive loop pattern (rise dynamics) at intermediate time scales between the fast and slow capacitive decays. Characteristic parameters during relaxations are indicated in these apparently different procedures but with similar time scales.

fascinating scenario in which some mechanisms could be “invisible” in impedance measurements but accessible in the time domain and vice versa. In the next section, an updated and summarized list of the time constants depending on the type of transient response (CLC or CCL) will be captured.

Figure 4 shows a representative transient-current response for our perovskite device under study in response to a small voltage perturbation of 10 mV (V_{app}) over a dc steady-state of 1 V. In a general view of the resulting transient, one simply visualizes a time decay. However, the current response contains much more complex dynamics at intermediate time scales, schematically zoomed in on the top of Figure 4. When the applied bias voltage is sufficiently high, the inductor is stimulated, and consequently, the transient dynamics exhibits, after the classical dielectric capacitive charge (nearly invisible due to ultra-fast timescales), additional features: The current increases at intermediate time scales and finally decreases, representing the charge processes of the chemical inductor and the interfacial capacitance, respectively (CLC). In effect, it exists a plausible connection between the two types of electrical signals, admittance - Figure 3, equivalent to Figure 2a - and the transient current, in terms of resistances and time constants, with the overall values calculated from the fittings of the immittance and transient data: $R_s = 19.15 \Omega$, $C_g = 42.07 \text{ nF}$, $R_b = 139.86 \Omega$, $R_x = 1.16 \text{ k}\Omega$, $C_x = 21.09 \mu\text{F}$, $\tau_L = 0.14 \text{ ms}$, and $L_a = 0.21 \text{ H}$. Next, we propose to develop a rationalized physical model for this type of universal transient response that involves inductive features at intermediate or long-time scales.

2.3. Mathematical Model to Interpret Time Transients in Metal Halide Perovskites

In **Figure 5a**, we show characteristic admittance spectra of metal halide perovskites equivalent to impedance forms extensively reported by many authors for multiple different application fields in recent years.^[15,18,26,44,61–63] The different shapes, now with the implicit frequency clockwise increasing (as in Figure 3), are obtained by numerical simulations and the variation of the value of

the characteristic time constants. For these parameters varying from small to large, we obtain an inductive loop or spiral structure at intermediate frequencies, the characteristic hook in the fourth quadrant of the complex admittance plane associated with a chemical inductor, or a double capacitive semicircle that finalizes with inductive traces (curl-back). By considering linear and time-invariant circuit theory^[64,65] and electrical processes sufficiently separated in frequency-domain, any resulting transient current can be expressed, in a clear and simple manner, as:

$$\Delta j(t) = \frac{V_{app}}{R_{dc}} + V_{app} \sum_{k=1}^N \left(\frac{1}{R_k} - \frac{1}{R_{k+1}} \right) \exp \left[-\frac{t}{\tau_k} \right] \quad (10)$$

where N represents the number of processes visualized in the complex plane representation, and R_k and τ_k are the initial resistance and the characteristic time scale for the relaxation process k . Note that in the vast majority of spectra in metal halide perovskites $N = 3$,^[18,41] being $\tau_1 = \tau_{ST}$, $\tau_2 = \tau_{MT}$, $\tau_3 = \tau_{LT}$, and $R_{N+1} = R_{dc}$. Thus, Equation (10) is a general expression that can be very useful to model any type of transient response of perovskite semiconductors under small signal conditions. If $R_{k+1} > R_k$, then the k -th exponential term is decreasing, indicative of a capacitive process. Otherwise, if $R_{k+1} < R_k$, then the corresponding current increases with time and one obtains a negative capacitance feature, which has been widely recognized in electronic systems with recombination governed by trap-mediated processes.^[66,67] This decrease (increase) of resistance (current) is due to the activation of the chemical inductor line when the bias voltage is high.^[68] For all these reasons, we numbered the characteristic frequencies and the associated resistances in the limiting cases corresponding to each arc of the Nyquist plots shown in Figure 5a. In order to obtain an analytical current response for the general case of metal halide perovskite devices, it is only necessary to adequately find the resistances. The code of colors and general properties of the characteristic time scales and resistances, by considering the cases of the chemical inductor in CLC and CCL configuration, are summarized in **Table 1**. For the case of the inductive loop under study here, our model provides an excellent agreement between the theory and the experimental data (refer to Figure 4). It is important to remark that the difference between the two cases lies in the manner of activation and deactivation of the capacitors and inductors once they have already emerged or not in the electrical response.

To further clarify the situation, Figure 5b shows all the respective transient dynamics, in logarithm-scaled times representation, for the immittance spectra of Figure 5a, with multiple spikes that separate the electrical processes. These components occurred at the instant $t_{spike,k}$, corresponding to the times when the step response changes the trend. Its value can be obtained by neglecting terms in different time scales and later taking the first-order derivative of $\Delta j(t)$ and setting it equal to zero: $d(\Delta j(t))/dt|_{t=t_{spike,k}} = 0$.^[69] That is, if one wants to calculate $t_{spike,1}$, it can be considered that $(1/R_3 - 1/R_{dc})\exp[-t/\tau_3] \rightarrow 0$ and, if on the contrary, the objective is to obtain $t_{spike,2}$, one can likewise assume that $(1/R_1 - 1/R_2)\exp[-t/\tau_1] \rightarrow 0$. Note that constant terms (partial or final dc steady-states) have no impact

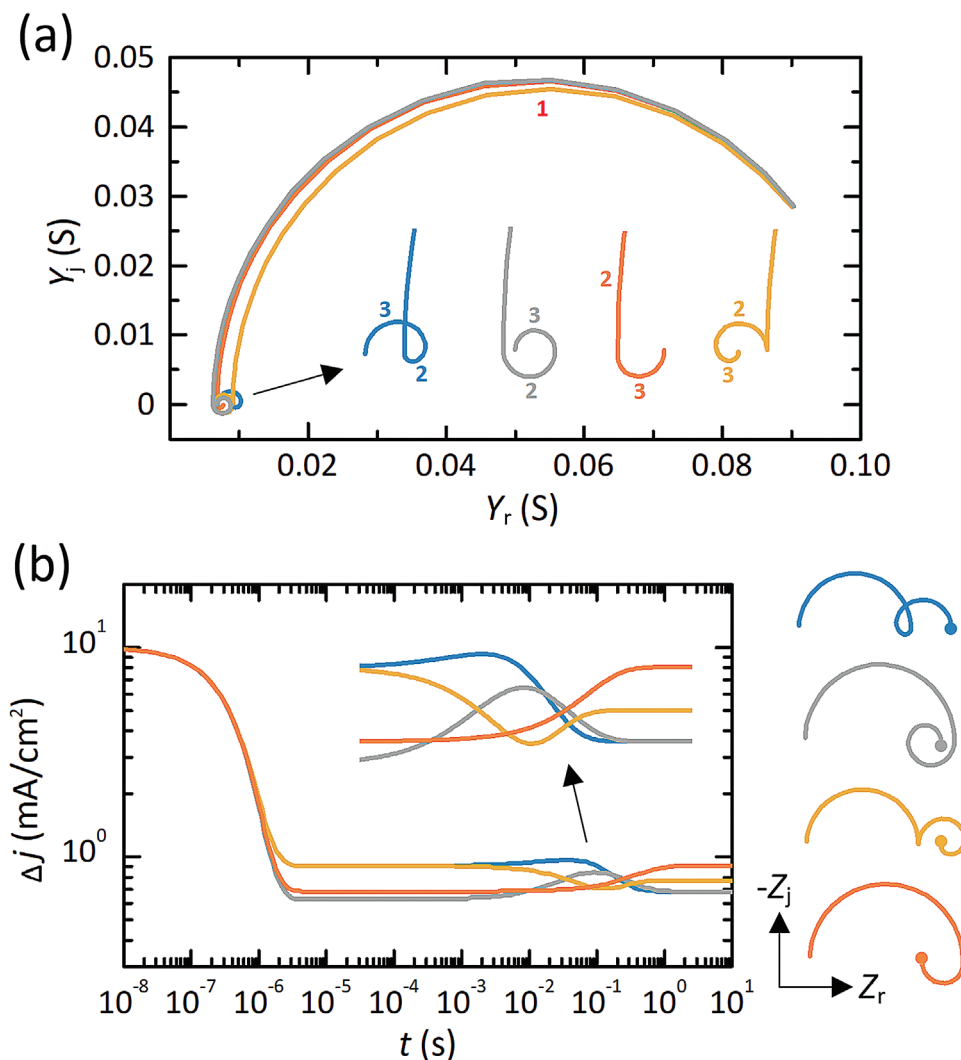


Figure 5. a) Numerical simulations of typical complex plane admittance plots in all types of perovskite semiconductors (e.g., solar cells, photodetectors, light-emitting diodes, and memristors) obtained for different kinetic relaxation constants and applied voltage biases by using the following values for the electrical elements of $R_s = 10 \Omega$, $C_g = 50 \text{ nF}$, $R_b = 300 \Omega$ and the other ones $\{R_x, C_x, R_a, L_a\}$ as $\{150 \Omega, 0.8 \text{ mF}, 250 \Omega, 10 \text{ H}\}$, $\{300 \Omega, 0.8 \text{ mF}, 250 \Omega, 10 \text{ H}\}$, $\{250 \Omega, 1 \text{ mF}, 150 \Omega, 50 \text{ H}\}$, or $\{150 \Omega, 0.4 \text{ mF}, 200 \Omega, 25 \text{ H}\}$ for the impedance patterns consisting of the inductive loop at intermediate frequencies, the spiral, the ideal chemical inductor structure, or the double capacitive arc that finalizes with inductive traces, respectively. Note that the processes have been numbered according to the order of appearance. b) Equivalent current transients in response to a voltage step of 10 mV exhibit a wide variety of dynamics with decays (capacitances), rises (inductors), and spike components. Next, we indicate the characteristic parameters obtained from Equations (11) and (12): $t_{\text{spike},1} = 7.32 \mu\text{s}$ and $t_{\text{spike},2} = 33.79 \text{ ms}$ for the inductive loop; $t_{\text{spike}} = 8.11 \mu\text{s}$ and $M_p = -24.65\%$ for the hook feature; $t_{\text{spike},1} = 7.31 \mu\text{s}$, $t_{\text{spike},2} = 0.10 \text{ s}$, and $M_p = -8.52\%$ for the inductive characteristic with a spiral trajectory; and $t_{\text{spike}} = 0.11 \text{ s}$ and $M_p = -15.38\%$ for the curl-back consisting of double capacitive arc that finalizes in a chemical inductor. Note that all these values provide excellent agreement with the simulation data. As a guide, impedance plots are also represented, where the dc conditions are marked by colored points.

Table 1. General model parameters of the time transient response depending on the inductive spectral pattern in the complex plane admittance representation.

Inductive feature	Code	τ_1	τ_2	τ_3	R_1	R_2	R_3	R_4
CLC: Loop or spiral	Blue	$R_s C_g$	$\frac{L_a}{R_a}$	$R_x C_x$	R_s	$R_s + \frac{R_b R_x}{R_b + R_x}$	$R_s + \left(\frac{1}{R_b} + \frac{1}{R_x} + \frac{1}{R_a}\right)^{-1}$	$R_s + \frac{R_a R_b}{R_a + R_b}$
CCL: Hook or curl-back	Orange		$R_x C_x$	$\frac{L_a}{R_a}$				

on obtaining $t_{\text{spike},k}$. With all that, a generalized spike time can be found in terms of the equivalent circuit elements as:

$$t_{\text{spike},k} = \frac{\ln \left[\frac{\tau_{k+1} R_{k+2} (R_k - R_{k+1})}{\tau_k R_k (R_{k+2} - R_{k+1})} \right]}{\tau_k^{-1} - \tau_{k+1}^{-1}} \quad (11)$$

Although this is not the case in this work, it is necessary to remember that the fast and intermediate processes for both cases of the CCL configurations in immittance spectra are capacitive in nature; thus, there is only one spike time. This last case is approximately equivalent to the analysis carried out in a previous work on the authors.^[27] Finally, one can obtain the negative percent overshoots, measured from the dc steady-state, according to the equation:

$$M_p = - \left(1 - \frac{R_{dc}}{R_{max}} \right) \times 100\% \quad (12)$$

where R_{max} is the maximum resistance estimated by Impedance Spectroscopy. Note that, logically, the negative overshoots do not apply to inductive loops ($R_{dc} = R_{max}$). Using Equations (11) and (12), we obtain the following values for the spike times in the experimental transient current response shown in Figure 4: $t_{\text{spike},1} = 7.83 \mu\text{s}$ and $t_{\text{spike},2} = 0.69 \text{ ms}$. To finalize, we should therefore indicate that, although Equations (11) and (12) are obviously numerical approximations, these relationships work well in the representative example under study, obtaining reasonable spike times and magnitudes of the minimum value, experimentally estimated, by inspection, from the inset of Figure 4.

Now that we have completed the description of theory and experimental measurements let us discuss the significance of our model for a better understanding of the practical application. As with impedance, the evolution of the voltage-dependent dynamics of transient currents also provides valuable information for establishing the physical origin of the electrical parameters that constitute an equivalent model. From the spectral patterns and the value of the characteristic circuit elements, the transient model could be able to establish, for instance, correlations in terms of perovskite chemistry (A-site & B-site variations, ionic vacancies, or deep-level defects).^[70-72] Nevertheless, it is advisable to use a combination of techniques under the same conditions to provide complementary understanding and more detailed information on the metal halide perovskites phenomenology due to the complexity of the electrical models depending on the myriad forms of active layer composition or the nature of the contact materials.^[18,73] As a result, the techniques under study here do not always provide universally accepted information itself in terms of chemical parameters and physical events, making it challenging to extract general conclusions.

Although current transient techniques under study here are of immense interest to the perovskite community due to numerous advantages previously indicated, it is important to note that, however, specific requirements of practical implementation in terms of voltage change time and sampling rate should be fulfilled, commonly by using expensive equipment, to completely capture the dynamical behavior of the transient responses exhibiting well-separated time scales. Furthermore, theoretical approaches to model transient dynamics can be perceived as highly

complicated because they require a certain mathematical background and having learned basic circuit theory concepts.

3. Conclusion

In conclusion, we presented the results of inductive loops in impedance measurements of metal halide perovskite materials and the corresponding current transient responses with complex multi-timescale dynamics. The phenomenological coupling of mechanisms of ionic and electronic nature, widely studied in the frequency domain, generates these new transient properties in perovskite semiconductors that require a dynamical model to adequately describe them. In this sense, we here explain the multiple changes from decay to rise transient dynamics and vice versa by the dominance of dielectric capacitance, chemical inductor, or light-enhanced capacitance for the case of the impedance spectra with inductive loop traces found in perovskite solar cells. To finalize, the present work provides a general guideline for the interpretation of current transient responses with mixed capacitive-inductive dynamics. The application of our mathematical approach is important because it enables a description of multiple transient processes, in which ionic conductance introduces a delay effect on the electronic processes, observed in different research disciplines (basic electrochemical systems, batteries, fuel cells, supercapacitors, solar cells, photodetectors, light-emitting diodes or memristors).

Supporting Information

Supporting Information is available from the Wiley Online Library or from the author.

Acknowledgements

This work has received funding from the Universidad Rey Juan Carlos, project number M2993. This work was also supported with funding from the European Research Council via the Advanced Grant 101097688 (PeroSpiker).

Conflict of Interest

The authors declare no conflict of interest.

Data Availability Statement

The data that support the findings of this study are available from the corresponding author upon reasonable request.

Keywords

halide perovskites, impedance spectroscopy, inductive loops, negative overshoots, transient analysis

Received: July 25, 2023
Revised: October 3, 2023
Published online: October 30, 2023

- [1] Y. Fu, H. Zhu, J. Chen, M. P. Hautzinger, X.-Y. Zhu, S. Jin, *Nat. Rev. Mater.* **2019**, 4, 169.
- [2] Z. Xiao, Y. Yuan, Y. Shao, Q. Wang, Q. Dong, C. Bi, P. Sharma, A. Gruverman, J. Huang, *Nat. Mater.* **2015**, 14, 193.
- [3] W. Tress, N. Marinova, T. Moehl, S. M. Zakeeruddin, M. K. Nazeeruddin, M. Grätzel, *Energy Environ. Sci.* **2015**, 8, 995.
- [4] K. Sakhatykyi, R. A. John, A. Guerrero, S. Tsarev, S. Sabisch, T. Das, G. J. Matt, S. Yakunin, I. Cherniukh, M. Kotyrba, Y. Berezovska, M. I. Bodnarchuk, S. Chakraborty, J. Bisquert, M. V. Kovalenko, *ACS Energy Lett.* **2022**, 7, 3401.
- [5] D. W. Dequillettes, W. Zhang, V. M. Burlakov, D. J. Graham, T. Leijtens, A. Osherov, V. Bulovic, H. J. Snaith, D. S. Ginger, S. D. Stranks, *Nat. Commun.* **2016**, 7, 11683.
- [6] T. Zhang, C. Hu, S. Yang, *Small Methods* **2020**, 4, 1900552.
- [7] C. Wagner, *J. Phys. Chem. Solids* **1972**, 33, 1051.
- [8] H. Rickert in, in *Electrochemistry of Solids*, Springer Verlag, Berlin **1982**.
- [9] W. Weppner, R. A. Huggins, *Ann. Rev. Mater. Sci.* **1978**, 8, 269.
- [10] J. E. Bauerle, *J. Phys. Chem. Solids* **1969**, 30, 2657.
- [11] J. Jamnik, J. Maier, *Phys. Chem. Chem. Phys.* **2001**, 3, 1668.
- [12] A. Senocrate, J. Maier, *J. Am. Chem. Soc.* **2019**, 141, 8382.
- [13] A. Senocrate, I. Moudrakovski, G. Y. Kim, T.-Y. Yang, G. Gregori, M. Grätzel, J. Maier, *Angew. Chem., Int. Ed.* **2017**, 56, 7755.
- [14] T.-Y. Yang, G. Gregori, N. Pellet, M. Grätzel, J. Maier, *Angew. Chem., Int. Ed.* **2015**, 54, 7905.
- [15] A. Guerrero, J. Bisquert, G. Garcia-Belmonte, *Chem. Rev.* **2021**, 121, 14430.
- [16] A. Dualeh, T. Moehl, N. Tétreault, J. Teuscher, P. Gao, M. K. Nazeeruddin, M. Grätzel, *ACS Nano* **2014**, 8, 362.
- [17] S.-M. Yoo, S. J. Yoon, J. A. Anta, H. J. Lee, P. P. Boix, I. Mora-Seró, *Joule* **2019**, 3, 2535.
- [18] E. Von Hauff, D. Klotz, *J. Mater. Chem. C* **2022**, 10, 742.
- [19] A. Todinova, L. Contreras-Bernal, M. Salado, S. Ahmad, N. Morillo, J. Idígoras, J. A. Anta, *ChemElectroChem* **2017**, 4, 2891.
- [20] P. Calado, A. M. Telford, D. Bryant, X. Li, J. Nelson, B. C. O'regan, P. R. F. Barnes, *Nat. Commun.* **2016**, 7, 13831.
- [21] R. A. Belisle, W. H. Nguyen, A. R. Bowring, P. Calado, X. Li, S. J. C. Irvine, M. D. McGehee, P. R. F. Barnes, B. C. O'regan, *Energy Environ. Sci.* **2017**, 10, 192.
- [22] A. Pockett, M. J. Carnie, *ACS Energy Lett.* **2017**, 2, 1683.
- [23] A. Pockett, M. Spence, S. K. Thomas, D. Raptis, T. Watson, M. J. Carnie, *Sol. RRL* **2021**, 5, 2100159.
- [24] L. Krückemeier, B. Krogmeier, Z. Liu, U. Rau, T. Kirchartz, *Adv. Energy Mater.* **2021**, 11, 2003489.
- [25] S. E. J. O'kane, G. Richardson, A. Pockett, R. G. Niemann, J. M. Cave, N. Sakai, G. E. Eperon, H. J. Snaith, J. M. Foster, P. J. Cameron, A. B. Walker, *J. Mater. Chem. C* **2017**, 5, 452.
- [26] F. Ebadi, N. Taghavinia, R. Mohammadpour, A. Hagfeldt, W. Tress, *Nat. Commun.* **2019**, 10, 1574.
- [27] E. Hernández-Balaguera, J. Bisquert, *ACS Energy Lett.* **2022**, 7, 2602.
- [28] E. Barsoukov, J. R. Macdonald, in *Impedance Spectroscopy: Theory, Experiment, and Applications*, John Wiley & Sons, New Jersey **2005**.
- [29] S. Wang, J. Zhang, O. Gharbi, V. Vivier, M. Gao, M. E. Orazem, *Nat. Rev. Methods Primers* **2021**, 1, 41.
- [30] Y. V. Pershin, M. Di Ventra, *Adv. Phys.* **2011**, 60, 145.
- [31] H. J. Snaith, A. Abate, J. M. Ball, G. E. Eperon, T. Leijtens, N. K. Noel, S. D. Stranks, J. T.-W. Wang, K. Wojciechowski, W. Zhang, *J. Phys. Chem. Lett.* **2014**, 5, 1511.
- [32] H.-S. Kim, I.-H. Jang, N. Ahn, M. Choi, A. Guerrero, J. Bisquert, N.-G. Park, *J. Phys. Chem. Lett.* **2015**, 6, 4633.
- [33] E. Hernández-Balaguera, L. Muñoz-Díaz, C. Pereyra, M. Lira-Cantú, M. Najafi, Y. Galagan, *Mater. Today Energy* **2022**, 27, 101031.
- [34] J.-Q. Yang, R. Wang, Z.-P. Wang, Q.-Y. Ma, J.-Y. Mao, Y. Ren, X. Yang, Y. Zhou, S.-T. Han, *Nano Energy* **2020**, 74, 104828.
- [35] E. Hernández-Balaguera, L. Muñoz-Díaz, A. Bou, B. Romero, B. Ilyassov, A. Guerrero, J. Bisquert, *Neuromorph. Comput. Eng.* **2023**, 3, 024005.
- [36] J. Bisquert, A. Guerrero, *J. Am. Chem. Soc.* **2022**, 144, 5996.
- [37] S. K. Roy, M. E. Orazem, B. Tribollet, *J. Electrochem. Soc.* **2007**, 154, B1378.
- [38] B. P. Setzler, T. F. Fuller, *J. Electrochem. Soc.* **2015**, 162, F519.
- [39] H. Brandstätter, I. Hanzu, M. Wilkening, *Electrochim. Acta* **2016**, 207, 218.
- [40] D. Klotz, *Electrochem. Commun.* **2019**, 98, 58.
- [41] A. Guerrero, G. Garcia-Belmonte, I. Mora-Seró, J. Bisquert, Y. S. Kang, T. J. Jacobsson, J.-P. Correa-Baena, A. Hagfeldt, *J. Phys. Chem. C* **2016**, 120, 8023.
- [42] E. Ghahremanirad, A. Bou, S. Olyae, J. Bisquert, *J. Phys. Chem. Lett.* **2017**, 8, 1402.
- [43] F. Fabregat-Santiago, M. Kulbak, A. Zohar, M. Vallés-Pelarda, G. Hodes, D. Cahen, I. Mora-Seró, *ACS Energy Lett.* **2017**, 2, 2007.
- [44] M. T. Khan, P. Huang, A. Almohammed, S. Kazim, S. Ahmad, *iScience* **2021**, 24, 102024.
- [45] E. Hernández-Balaguera, B. Arredondo, C. Pereyra, M. Lira-Cantú, *J. Power Sources* **2023**, 560, 232614.
- [46] M. T. Neukom, A. Schiller, S. Züfle, E. Knapp, J. Ávila, D. Pérez-Del-Rey, C. Dreessen, K. P. S. Zaroni, M. Sessolo, H. J. Bolink, B. Ruhstaller, *ACS Appl. Mater. Interfaces* **2019**, 11, 23320.
- [47] B.-W. Park, N. Kedem, M. Kulbak, D. Y. Lee, W. S. Yang, N. J. Jeon, J. Seo, G. Kim, K. J. Kim, T. J. Shin, G. Hodes, D. Cahen, S. I. Seok, *Nat. Commun.* **2018**, 9, 3301.
- [48] H. Xie, Z. Wang, Z. Chen, C. Pereyra, M. Pols, K. Galkowski, M. Anaya, S. Fu, X. Jia, P. Tang, D. J. Kubicki, A. Agarwalla, H.-S. Kim, D. Prochowicz, X. Borrisé, M. Bonn, C. Bao, X. Sun, S. M. Zakeeruddin, L. Emsley, J. Arbiol, F. Gao, F. Fu, H. I. Wang, K.-J. Tielrooij, S. D. Stranks, S. Tao, M. Grätzel, A. Hagfeldt, M. Lira-Cantu, *Joule* **2021**, 5, 1246.
- [49] D. A. Jacobs, H. Shen, F. Pfeffer, J. Peng, T. P. White, F. J. Beck, K. R. Catchpole, *J. Appl. Phys.* **2018**, 124, 225702.
- [50] S. Ravishankar, A. Riquelme, S. K. Sarkar, M. Garcia-Batlle, G. Garcia-Belmonte, J. Bisquert, *J. Phys. Chem. C* **2019**, 123, 24995.
- [51] A. O. Alvarez, R. Arcas, C. A. Aranda, L. Bethencourt, E. Mas-Marzá, M. Saliba, F. Fabregat-Santiago, *J. Phys. Chem. Lett.* **2020**, 11, 8417.
- [52] J. Bisquert, *J. Phys. Chem. Lett.* **2023**, 14, 1014.
- [53] J. Bisquert, A. Guerrero, C. Gonzales, *ACS Phys. Chem Au* **2021**, 1, 25.
- [54] C. Gonzales, A. Guerrero, J. Bisquert, *J. Phys. Chem. C* **2022**, 126, 13560.
- [55] N. Filipoiu, A. T. Preda, D.-V. Anghel, R. Patru, R. E. Brophy, M. Kateb, C. Besleaga, A. G. Tomulescu, I. Pintilie, A. Manolescu, G. A. Nemnes, *Phys. Rev. Appl.* **2022**, 18, 064087.
- [56] E. Hernández-Balaguera, D. Martin-Martin, *Fractal Fract.* **2023**, 7, 516.
- [57] E. Hernández-Balaguera, B. Romero, M. Najafi, Y. Galagan, *Adv. Mater. Interfaces* **2022**, 9, 2102275.
- [58] R. S. Sanchez, V. Gonzalez-Pedro, J.-W. Lee, N.-G. Park, Y. S. Kang, I. Mora-Seró, J. Bisquert, *J. Phys. Chem. Lett.* **2014**, 5, 2357.
- [59] E. Hernández-Balaguera, B. Romero, B. Arredondo, G. Del Pozo, M. Najafi, Y. Galagan, *Nano Energy* **2020**, 78, 105398.
- [60] E. Hernández-Balaguera, G. Del Pozo, B. Arredondo, B. Romero, C. Pereyra, H. Xie, M. Lira-Cantú, *Sol. RRL* **2021**, 5, 2000707.
- [61] A. Pockett, G. E. Eperon, T. Peltola, H. J. Snaith, A. Walker, L. M. Peter, P. J. Cameron, *J. Phys. Chem. C* **2015**, 119, 3456.
- [62] D. Moia, I. Gelmetti, P. Calado, W. Fisher, M. Stringer, O. Game, Y. Hu, P. Docampo, D. Lidzey, E. Palomares, J. Nelson, P. R. F. Barnes, *Energy Environ. Sci.* **2019**, 12, 1296.

- [63] L. Contreras-Bernal, S. Ramos-Terrón, A. Riquelme, P. P. Boix, J. Idígoras, I. Mora-Seró, J. A. Anta, *J. Mater. Chem. A* **2019**, *7*, 12191.
- [64] J. W. Nilsson, S. Riedel, in *Electric Circuits*, Pearson, London, UK **2015**.
- [65] F. F. Kuo, in *Network Analysis and Synthesis*, John Wiley & Sons, New York, USA **1962**.
- [66] X. Wu, E. S. Yang, H. L. Evans, *J. Appl. Phys.* **1990**, *68*, 2845.
- [67] E. Ehrenfreund, C. Lungenschmied, G. Dennler, H. Neugebauer, N. S. Sariciftci, *Appl. Phys. Lett.* **2007**, *91*, 012112.
- [68] J. Bisquert, A. Bou, A. Guerrero, E. Hernández-Balaguera, *APL Mach. Learn.* **2023**, *1*, 036101.
- [69] K. Ogata, in *Modern Control Engineering*, Prentice Hall, Hoboken, New Jersey **2010**.
- [70] S. R. Raga, Y. Qi, *J. Phys. Chem. C* **2016**, *120*, 28519.
- [71] P. Srivastava, R. Kumar, M. Bag, *J. Phys. Chem. C* **2021**, *125*, 211.
- [72] C. Bao, F. Gao, *Rep. Prog. Phys.* **2022**, *85*, 096501.
- [73] A. Bou, A. Pockett, D. Raptis, T. Watson, M. J. Carnie, J. Bisquert, *J. Phys. Chem. Lett.* **2020**, *11*, 8654.